Correlation between texture, anisotropy, and vector magnetization processes investigated by two-dimensional vector vibrating sample magnetometry in $BaO(Fe_2O_3)_6$ thin film

P. R. Ohodnicki,[1,a)] K. Y. Goh,[1] M. E. McHenry,[1] K. Ziemer,[2] Z. Chen,[3] C. Vittoria,[3] and V. G. Harris[3]

[1]*Materials Science and Engineering Department, Carnegie Mellon University, Pittsburgh, Pennsylvania 15213, USA*

[2]*Department of Chemical Engineering, Northeastern University, Boston, Massachusetts 02115, USA*

[3]*Department of Electrical and Computer Engineering, Northeastern University, Boston, Massachusetts 02115, USA*

(Presented on 6 November 2007; received 23 August 2007; accepted 4 December 2007; published online 25 March 2008)

High ferromagnetic resonance frequencies and low linewidths in $BaO(Fe_2O_3)_6$ thin films are achieved by obtaining a low-dispersion of crystallite easy *c* axes normal to the film. X-ray diffraction and magnetic force microscopy are used to characterize texture and magnetic domain structure for a $BaO(Fe_2O_3)_6$ film deposited on (0001) SiC with a MgO (111) template layer. Strong *c*-axis texture normal to the film is observed resulting in strong uniaxial anisotropy. The consequent vector magnetization processes due to a combination of domain wall motion and magnetization rotation are characterized by two dimensional vector coil vibrating sample magnetometry (VVSM).

[DOI: 10.1063/1.2838630]

M-type $BaO(Fe_2O_3)_6$ (BaM) is an important high-frequency microwave (μ-wave) material due to a strong uniaxial magnetocrystalline anisotropy, $K_{Ucrystal}$. For propagation of electromagnetic (EM) waves in many μ-wave device applications, the easy axis should be oriented normal to the film.[1–4] Here, the texture of a 300–400 nm $BaO(Fe_2O_3)_6$ thin film deposited on MgO (111) on SiC(0001) discussed in Ref. 5 is characterized by x-ray diffraction (XRD) and analyzed with a simple model to estimate the effect of measured *c*-axis dispersion on the film anisotropy. Strong uniaxial anisotropy results in a striped magnetic domain structure and vector magnetization processes which are characterized by magnetic force microscopy (MFM) and two-dimensional (2D) vector coil vibrating sample magnetometry (VVSM).

6*H*-SiC (0001) single crystal wafers were cleaned in a custom-built hydrogen furnace and a 10 nm crystalline MgO (111) film was grown by molecular beam epitaxy (MBE) at ~150 °C using a low-temperature Mg effusion cell and a remote oxygen plasma source.[6,7] The sample was immediately transferred to the pulsed laser deposition (PLD) chamber for deposition of $BaO(Fe_2O_3)_6$ by a Tui KrF Excimer laser. Specific details of the growth can be found in Refs. 3 and 8.

The BaM hexaferrite orientation was determined from x-ray pole figures taken using CuK_α radiation on a Philips high resolution x-ray diffractometer.[4,5] 2D magnetization trajectories (M_x parallel and M_y perpendicular to field) were obtained using a Lakeshore VVSM. The magnitude of the torque is equal to the magnetization component perpendicular to the field multiplied by the applied field magnitude ($|\tau| = |M_{\perp H} H|$). For samples with symmetry such that the magnetization component normal to both sensing coils is negligible ($M_z = 0$), $M_{\perp H} = M_y$, the magnetization process is 2D, and torque magnetometry can be performed with 2D VVSM. This symmetry is confirmed here from pole figures.

Figure 1 shows pole figures for values of $2\theta \sim 23.03$ and 30.30° corresponding to (006) and (110) reflections, respectively. The sharp peak at the center of the (006) pole figure indicates excellent *c*-axis alignment normal to the film. The sixfold symmetry of intensity due to the similar *d*-spacings of {104} planes with the (006) planes indicates in-plane epitaxy between BaM and the MgO layer as indexed in Fig. 1(a). Quantitative analysis of the (006) pole figures[4] suggests that >98% of the BaM grains have easy axes within 5° of the film normal. The dashed line in Figs. 1(a) and 1(b) show the rotation axis of the sample in experiments discussed below. A mirror plane normal to this rotation axis observed in the pole figures satisfies the symmetry requirement for $M_Z = 0$ and $M_{\perp H} = M_y$.

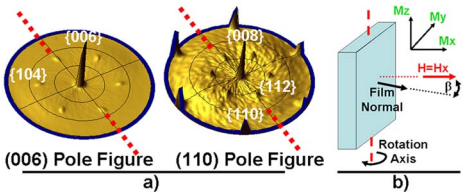

FIG. 1. (Color online) (a) Pole figures obtained for $2\theta \sim 23.03$ and 30.30 displaying *c*-axis texture normal to the film surface and in-plane expitaxy. (b) Schematic for the rotation experiments (thick dashed line=rotation axis). β=misorientation between film normal and applied field.

[a)]Author to whom correspondence should be addressed. Electronic mail: pohodnic@andrew.cmu.edu.

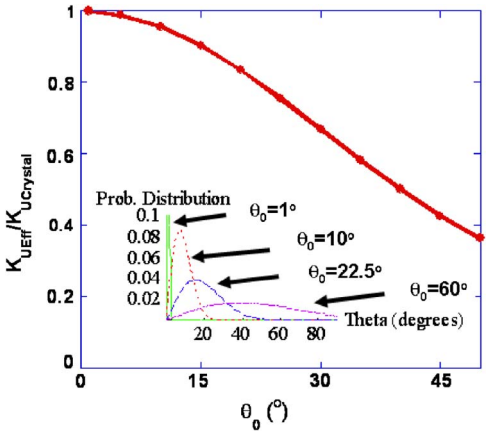

FIG. 2. (Color online) Effective magnetocrystalline anisotropy of the aggregate of grains as a function of the *c*-axis dispersion for a Gaussian-like distribution of grain orientations defined in Eq. (2).

The *c*-axis dispersion dictates the effective anisotropy of the film and the quantitative results of the pole figures can be used to estimate the magnitude. The effective magnetocrystalline anisotropy energy of a saturated film, given a probability distribution of the c-axis orientations with respect to the film normal in spherical coordinates, is

$$E_A(\theta',\phi') = \int_{\phi=0}^{\phi=2\pi}\int_{\theta=0}^{\theta=\pi/2} \rho(\theta,\phi)K_{\text{Ucrystal}} \times \sin^2[\varpi(\theta,\phi,\theta',\phi')]d\theta d\phi, \quad (1)$$

where $\rho(\theta,\phi)$ can be determined from pole figures. It represents the volume fraction probability distribution of grains with easy axes lying between $\theta+d\theta$ and $\phi+d\phi$. θ and θ' are the angles between the film normal and the *c* axis of a given grain or the film magnetization, respectively. ϕ and ϕ' are the corresponding azimuthal angles. K_{Ucrystal} is the uniaxial anisotropy constant of the BaM crystallites, and $\varpi(\theta,\phi,\theta',\phi')$ is the angle between the film magnetization defined by ϕ' and θ' and grains with *c* axes along the direction defined by ϕ and θ.

To simplify the analysis, we neglect the observed in-plane texture and assume a Gaussian-like distribution of the easy axes with respect to the film normal:

$$\rho(\theta,\phi) \rightarrow \rho(\theta) = \rho_0 e^{-(\theta/\theta_0)^2} \sin\theta, \quad (2)$$

where ρ_0 is a normalization constant and θ_0 is a measure of the angular deviation of *c*-axis orientations from the film normal. Larger values of θ_0 correspond to greater *c*-axis dispersion.

Figure 2 shows the assumed probability distribution of grain orientations for several values of θ_0 using Eq. (2) and the effective magnetocrystalline anisotropy, K_{Ueff}, for the aggregate of grains relative to K_{Ucrystal} of each grain. K_{Ueff} is defined here as the peak of torque curves simulated from Eq. (1) according to $\tau=-\partial E_A/\partial\theta$ using the distribution function in Eq. (2). For larger θ_0 values, the distribution approaches random and K_{Ueff} approaches zero. In our film the probability distribution approximates $\theta_0<5°$ as 98% of grains have *c* axes oriented within 5° of the film normal. The *c*-axis dispersion is not expected to significantly impact the effective film anisotropy.

The *c*-axis texture results in the strong uniaxial anisotropy normal to the film surface evident in the M_X hysteresis loops in Fig. 3(a). The misorientation angle between the film normal and the applied magnetic field is represented by the angle β as defined in Fig. 1(b). An easy axis loop is observed for $\beta=0°$ ($H\|\langle 001\rangle$, out of plane) and a hard axis loop is observed for $\beta=90°$ ($H\|\langle 110\rangle$, in plane). Fig. 3(a) illustrates that M_y is zero throughout the magnetization process for $\beta=0°$ indicating that the magnetization process is scalar. The anisotropy field (H_K) of the film is larger than 1 T, the maximum field for the VVSM setup used here.

Figure 3(b) shows the M_X and M_y hysteresis loops for $\beta=45°$ and a vector magnetization process is observed ($M_y\neq 0$). Torque per unit volume, τ, is also plotted in Fig. 3(b). For $\beta=45°$, both M_y and τ are hysteretic with the torque reversing sign in a narrow field range near the film coercivity. At the highest fields, M_y decreases with H and the torque approaches saturation. However, the maximum field that can be applied ($H=1$ T) was insufficient to saturate the film for fields at 45° to the easy axis and thus anisotropy coefficients estimated from the measured torque are underestimated as in Ref. 4. The film exhibits an irregular striped magnetic domain structure ~200–300 nm in width with magnetization normal to the film as observed in MFM data of Fig. 3(c).

To better understand the vector magnetization process for arbitrary β, 2D magnetization trajectories were measured. In the first experiments, β was varied over a 360° range and back by rotating the sample in a field of fixed magnitude and direction about the dashed line of Fig. 1(c). These rotation experiments have the same geometry as standard rotational hysteresis or conventional torque experiments. In a second set, M_x and M_y hysteresis loops were obtained by varying H for fixed β. Both sets of experiments were performed after applying and subsequently removing a saturating 1 T field along the easy axis to return it to the remanent state. Experiments were performed under identical initial conditions be-

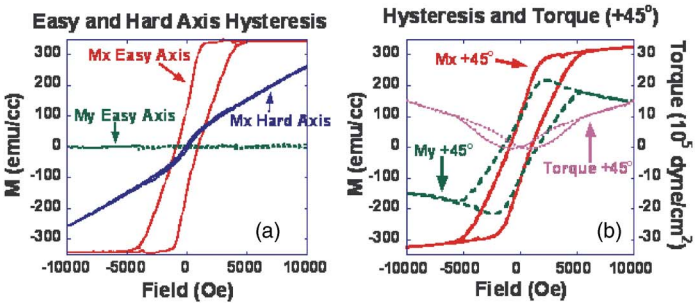

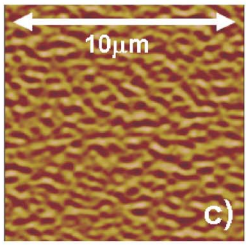

FIG. 3. (Color online) Easy and hard axis *Mx* and *My* hysteresis loops (a) and *Mx*, *My*, and torque for magnetization with fields applied at 45° to the easy axis (b). In (c), an irregular striped domain structure is observed with magnetization normal to the film. The hysteresis loops were not corrected for demagnetizing field effects.

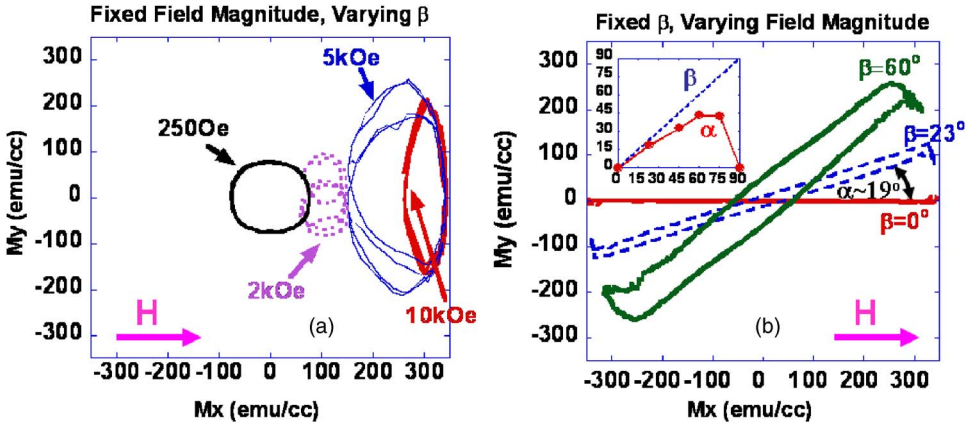

FIG. 4. (Color online) 2D magnetization trajectories for (a) rotational hysteresis experiments obtained for varying β in fixed applied fields along the positive x direction and (b) standard hysteresis experiments for fixed β and varying field magnitude and sign along the x axis. The inset in (b) illustrates the angle of inclination of the low-field magnetization trajectory, α, as a function of the easy axis orientation, β. Both are measured with respect to the applied field direction.

cause the films are strongly hysteretic. Demagnetization corrections were not performed as they are more complicated in the case of vector magnetization as opposed to scalar magnetization processes.[9]

Figure 4(a) shows three regimes of the magnetization trajectory during rotation experiments (fixed H, varying β). In Fig. 4(a), H is fixed in magnitude and direction along the $+x$ axis. For the largest fields (e.g., $H=10$ kOe), rotational magnetization trajectories are "lens" shaped indicating that the magnetization vector oscillates about the field direction due to the torque exerted by the effective film anisotropy. In this field range, the maximum value of M_y decreases with increasing field strength. At intermediate fields ($H=2$ and 5 kOe), irreversible domain wall processes result in trajectories with two separate branches. The smallest applied fields (e.g., $H=250$ Oe) are insufficient to activate irreversible domain wall processes and the remanent magnetization is approximately fixed along the easy axis and rotates with the sample.

Plots of M_y and τ as a function of β analogous to measurements using standard torque magnetometers are acquired simultaneously using VVSM. For brevity, the results are not presented but they also exhibit three different regimes. For high fields (e.g., $H\sim10$ kOe), M_y and τ as a function of angle are reversible with a period of $\Delta\beta=180°$ corresponding to the "lens shaped" trajectories of Fig. 4(a). For intermediate fields (e.g., $H\sim2$ and 5 kOe), hysteresis in both M_y and τ are observed corresponding to the branched trajectories of Fig. 4(a). For low fields (e.g., $H\sim250$ Oe), M_y and τ are reversible but with a longer period of $\Delta\beta=360°$ corresponding to rotation of the remanent magnetization with the sample as in Fig. 4(a).

Figure 4(b) shows the magnetization trajectory for hysteresis loops measured at fixed β with a varying H that is fixed along the x axis. For $\beta=0$, a scalar magnetization process is observed (e.g., $M_y=0$) because H is along the easy axis as in the hysteresis loop of Fig. 3(a). For nonzero β, two principal regimes are observed in the vector magnetization process. At the lowest fields, a linear trajectory with hysteresis is observed. The inclination of this low-field linear trajectory with respect to the field is indicated by α, as illustrated on Fig. 4(b) for $\beta=23°$. At the highest applied fields, a reversible portion of the magnetization trajectory with different slope is observed.

The low-field hysteretic regime is associated with domain wall motion and the reversible high-field regime is dominated by rotational processes. However, it is observed that $\alpha<\beta$ for $\beta>0°$ indicating that the low-field trajectory is not precisely parallel to the easy axis orientation for finite β as would be expected for pure domain wall motion. This is shown in the inset of Fig. 4(b) which indicates the magnetization process to be a combination of domain wall motion and rotation even in low fields. As β increases up to $\beta\sim60°-70°$, α also increases but at a decreasing rate indicating rotation to become more significant. For $\beta>\sim60°-70°$, the low-field trajectory is nonlinear and deviates strongly from the easy axis orientation until the magnetization process again becomes scalar along the hard axis (i.e., $\alpha=0°$ for $\beta=90°$). The sharp drop in α for $\beta>\sim60°-70°$ [see inset of Fig. 4(b)] indicates that rotation becomes the dominant magnetization mechanism. The relative importance of domain wall motion and magnetization rotation depends on the magnitude of the applied field and the misorientation between the applied field and the film normal.

A model has been presented to estimate the effect of the c-axis dispersion on the effective uniaxial anisotropy of a BaM/MgO/SiC film based on a distribution function measured directly by spherical integration of pole figures. Excellent c-axis texture normal to the film results in a strong uniaxial anisotropy, an irregular striped domain structure, and vector magnetization processes. Hysteresis and rotational hysteresis experiments indicate the dominant magnetization mechanism to depend on both the field magnitude and its misorientation with the easy axis. The VVSM technique allows one to characterize vector magnetization processes better than single coil VSM or conventional torque magnetometers alone.

[1]J. D. Adam *et al.*, IEEE Trans. Microwave Theory Tech. **50**, 721 (2002).
[2]Y. Chen *et al.*, Appl. Phys. Lett. **88**, 062516 (2006).
[3]Z. Chen *et al.*, J. Magn. Magn. Mater. **301**, 166 (2006).
[4]P. R. Ohodnicki *et al.*, J. Appl. Phys. **101**, 09M521 (2007).
[5]Z. Chen *et al.*, Appl. Phys. Lett. **91**, 182505 (2007).
[6]T. L. Goodrich, J. Parisi, Z. Cai, and K. S. Ziemer, Appl. Phys. Lett. **90**, 042910 (2007).
[7]T. L. Goodrich, Z. Chen, M. D. Losego, J.-P. Maria, and K. S. Ziemer, J. Vac. Sci. Technol. B **25**, 1033 (2007).
[8]Z. Cai, Z. Chen, T. L. Goodrich, V. G. Harris, and K. S. Ziemer, J. Cryst. Growth (in press).
[9]K. Ouchi and S. Iwasaki, IEEE Trans. Magn. **24**, 3009 (1988).